

# RadAlign: Advancing Radiology Report Generation with Vision-Language Concept Alignment

Difei Gu, Yunhe Gao, Yang Zhou, Mu Zhou, and Dimitris Metaxas

Rutgers University

**Abstract.** Automated chest radiographs interpretation requires both accurate disease classification and detailed radiology report generation, presenting a significant challenge in the clinical workflow. Current approaches either focus on classification accuracy at the expense of interpretability or generate detailed but potentially unreliable reports through image captioning techniques. In this study, we present RadAlign, a novel framework that combines the predictive accuracy of vision-language models (VLMs) with the reasoning capabilities of large language models (LLMs). Inspired by the radiologist’s workflow, RadAlign first employs a specialized VLM to align visual features with key medical concepts, achieving superior disease classification with an average AUC of 0.885 across multiple diseases. These recognized medical conditions, represented as text-based concepts in the aligned visual-language space, are then used to prompt LLM-based report generation. Enhanced by a retrieval-augmented generation mechanism that grounds outputs in similar historical cases, RadAlign delivers superior report quality with a GREEN score of 0.678, outperforming state-of-the-art methods’ 0.634. Our framework maintains strong clinical interpretability while reducing hallucinations, advancing automated medical imaging and report analysis through integrated predictive and generative AI. Code is available at <https://github.com/difeigu/RadAlign>.

**Keywords:** Vision-Language Model · Visual Concept Learning · Radiology Report Generation.

## 1 Introduction

Medical image interpretation and report generation play a vital role in the clinical workflow that can directly impact disease characterization and patient care [14]. The accurate interpretation of chest radiographs remains a critical task in medical image assessment [16], where clinicians must recognize subtle abnormalities and translate these observations into precise disease classifications and detailed reports. Accomplishing this complex task requires systematic efforts to capture a detailed state of the disease and to generate comprehensive, well-reasoned explanations of these findings [24].

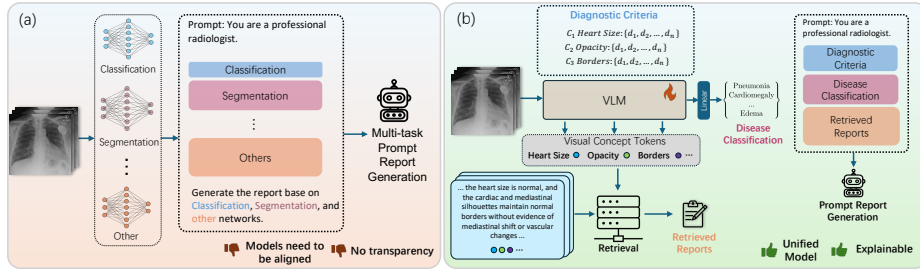


**Fig. 1.** (a) State-of-the-art report generation models such as ChatCAD aggregate predictions from multiple models. This approach can often cause inconsistencies in the generated reports. (b) Inspired by the diagnostic process of radiologists, our RadAlign combines disease classification, disease concepts, past report cases, and LLM’s strong reasoning capabilities to produce clinically coherent reports.

Current research on chest radiographic interpretation has developed primarily into classification models and image captioning approaches. First, classification methods build on deep convolutional neural networks [9,2,31] and vision transformers [8,20,17] have shown impressive diagnostic precision in detecting various conditions such as pneumonia, cardiomegaly, and pulmonary edema. However, these models operate as black boxes, providing only disease labels without explaining the visual features or solid reasoning that led to their predictions. This poor lack of interpretability limits their clinical utility in the real world, as healthcare providers always need to understand the basis for diagnostic decision making. Second, growing efforts have investigated image captioning approaches [11,6] [26,1] towards generating detailed open-text radiology reports. Although these methods can produce human-readable reports, they often suffer from hallucination—generating incorrect or unreliable information misaligned with the actual image content or medical knowledge [23].

Recent advances in large language models (LLMs) [4,7,25] and vision-language models (VLMs) [22,3,13] have opened new possibilities for medical image analysis. However, directly applying these models to chest X-ray interpretation presents significant challenges. While LLMs excel at natural language generation, they can produce unreliable medical information without proper grounding in visual evidence [28]. Similarly, existing VLMs [22,3,13] trained on natural images often lack the specific medical knowledge required for accurate diagnosis, necessitating domain-specific adaptation [3,29]. Recent attempts have addressed these limitations by using multiple models. For instance, ChatCAD [27], combines multi-component classification networks, segmentation models, report generation models, and LLMs. While ChatCAD leverages diverse model capabilities, it introduces computational redundancy and integration challenges. The lack of coherent alignment between these components can lead to inconsistencies between individual model predictions and the final generated reports, potentially compromising the reliability of the overall system.

To bridge this gap, we draw inspiration from the systematic approach that is routinely used by radiologists in clinical practice. Expert radiologists typically follow a structured process for image assessment and report generation. They first assess specific diagnostic criteria and medical concepts (such as heart size, lung opacity, pulmonary vessels, or pleural effusions) and then synthesize these observations with their medical knowledge to form the diagnoses and detailed reports. This key observation motivates our development of **RadAlign**, a novel framework that unifies the strengths of predictive models with the reasoning capabilities of LLMs. Unlike prior approaches that treat visual analysis and report generation as separate tasks, RadAlign creates a seamless pipeline that purposely mirrors the radiologist’s workflow on the concept-based image diagnosis.

RadAlign introduces three key contributions: First, it employs a vision-language model specifically designed to align visual features with medical concepts, mirroring how radiologists identify diagnostic criteria. This alignment process ensures that the model learns to recognize clinically relevant features and their relationships to medical terminology. Second, it leverages this well-structured and aligned representation on medical concepts to prompt LLMs in generating detailed reports, combining the accuracy of predictive models with the expressive power of generative LLMs. Third, it incorporates a concept-based retrieval-augmented generation mechanism that enhances reliability by grounding LLM outputs in similar cases from validated training data. This comprehensive approach provides multiple merits. It enables both accurate disease classification and detailed report generation while maintaining clinical reliability. At its core, the VLM is trained to better align the visual features with medical concepts, and we can use the out-of-shelf LLMs without finetuning. Our method doesn’t need expensive training on the LLMs but can leverage their superior capability on editing and reasoning, as the visual-language alignment is done in the VLM.

Our main contributions are:

- A unified framework that bridges the gap between classification accuracy and detailed reporting through vision-language concept alignment.
- A novel approach to medical report generation that mirrors radiologist workflow, combining visual feature recognition with LLM-based reasoning.
- A retrieval-augmented generation system that enhances report reliability by grounding predictions in similar historical cases.
- Superior performance across both classification and report generation benchmarks, with improved interpretability for clinical applications.

## 2 Methodology

Fig. 2 illustrates the proposed RadAlign framework. We present the detailed steps of RadAlign, which involve querying knowledge as diagnostic criteria, align-

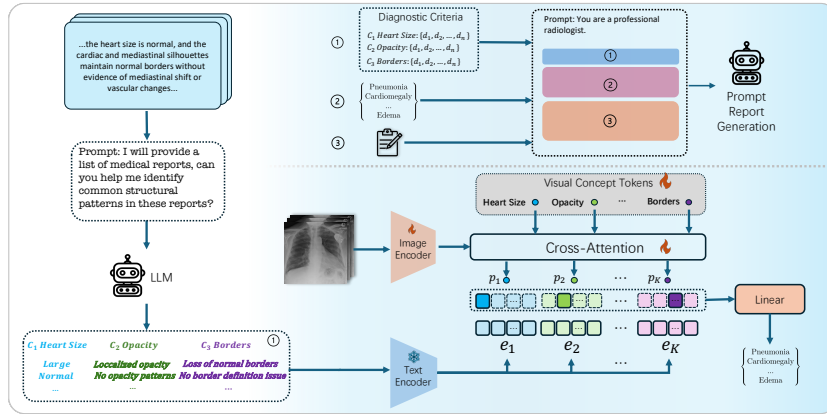


**Fig. 2.** An overview of RadAlign: The radiology report is generated via three unified components. Disease prediction through vision-language concept alignment and an explainable classifier; diagnostic criteria and medical concepts through LLM knowledge query; and retrieval-augmented historical reports cases from visual concept tokens.

ing visual features with these criteria, enabling report retrieval, and prompting an LLM for final report generation.

## 2.1 Domain Knowledge Query

Taking inspiration from human experts’ diagnoses, they observe different criteria that would help with the diagnosis through findings, then make informed judgments on the patient’s condition. We first extract diagnosis criteria through data-mining from the human expert findings. Let  $D = \{(x, P, y)\}$  be a set of training image-findings-label pairs, where  $x$  is the image,  $P$  is the ground truth findings from human experts, and  $y \in \mathcal{Y}$  is a label from a set of  $N$  disease classes. We use the training finding set  $\mathcal{P} = \{P_1, P_2, \dots, P_{|D|}\}$  and prompt LLM for a criteria extraction procedure  $f_e : \mathcal{P} \rightarrow \mathcal{C}$ , such that we get a  $K$  disentangled criteria axis set  $\{\mathcal{C}_i\}_{i=1}^K$ . For instance, in the case of chest x-ray, the criteria axis includes Heart Size, Lung Opacity, Diaphragm Position, Presence of Fluid, Borders of Cardiac/Mediastinal Silhouette. Subsequently, we query detailed knowledge on each of the criteria for each disease class with  $\mathcal{C}_i = \{C_i^1, C_i^2, \dots, C_i^{n_i}\}$ , where  $1 < n_i < N$  with each containing descriptions about the criteria regarding each of the  $N$  diseases. For example, the criteria axis Heart Size contains the description of ‘Enlargement of the heart silhouette’ for the disease Cardiomegaly, but ‘Does not affect the heart size’ for pneumonia, and ‘May or may not affect heart size depending on the cause’ for the other diseases. Additionally, we construct a mapping of disease ground truth for each of the concept descriptions  $f_m : \mathcal{C} \rightarrow \mathcal{Y}$ , i.e., for each concept axis, the description is paired with one or more disease classes. For instance, both normal and Cardiomegaly instances should have no influence on fluid accumulation. Therefore, they are both mapped to the ‘No fluid accumulation’ description.



## 2.2 Visual Concept Fine-grained Alignment

After constructing the lists for the diagnostic criteria axis, we aim to leverage its complex conceptual relationships for a more fine-grained alignment between visual features and concept features. Given a pretrained vision-language model containing a visual encoder  $\mathcal{V}$  and a textual encoder  $\mathcal{T}$ , we construct embedding for the diagnostic criteria. The textual criteria are initially encoded into criteria embedding anchors,  $\{\mathbf{e}_i = \mathcal{T}(C_i)\}_{i=1}^K$ , where  $\mathbf{e}_i \in \mathcal{R}^{n_i \times d}$ , and  $d$  is the dimension of the embedding. Intuitively, these textual embedding represents the sparse human knowledge that serves as anchors to facilitate informative vision feature learning and alignment.

To capture the visual concept, the visual concept learning module applies a set of  $K$  learnable visual concept tokens  $\mathbf{z} \in \mathcal{R}^{K \times d}$ . Given the image  $x$  and the feature map  $\mathcal{V}(x)$ , We use a cross-attention module to capture the nuanced features from a given image:

$$\hat{\mathbf{z}} = \text{cross-attention}(\mathbf{z}, \mathcal{V}(x), \mathcal{V}(x)), \quad (1)$$

Where  $\mathbf{z}$  is the query, and  $\mathcal{V}(x)$  is the key and value. The idea is for each of the  $K$  visual concept tokens to represent a criteria axis and capture a specific visual feature on the image that aligns with the concept.

We facilitate the learning of the visual encoder and visual concept tokens using domain-specific contrastive loss. For each criteria axis, we aggregate the concept tokens  $\hat{\mathbf{z}}$  and compare them against the corresponding criteria embedding anchors  $\mathbf{e}_i$  and compute a similarity score. The domain-specific contrastive loss is formulated as follows:

$$\mathcal{L}_{anchor}^i(\hat{\mathbf{z}}_i, \mathbf{e}_i) = -\log \frac{\exp(\text{sim}(\hat{\mathbf{z}}_i, \mathbf{e}_i^{\text{positive}}) / \tau)}{\sum_{j=1}^{n_i} \exp(\text{sim}(\hat{\mathbf{z}}_i, \mathbf{e}_i^j) / \tau)} \quad (2)$$

where  $\hat{\mathbf{z}}_i$  is the visual concept tokens,  $\mathbf{e}_i$  is the criteria embeddings, and  $\tau$  is the temperature parameter that adjusts the softness of the softmax distribution. We use dot product for cosine similarity. The utilization of the contrastive loss brings similar concepts  $\hat{\mathbf{z}}_i$  and  $\mathbf{e}_i$  together and pushes away dissimilar concepts. This process ensures more fine-grained learning from the model and helps become more discriminative when identifying the image. To do this, we optimize a joint objective comprising a criteria anchor contrastive loss with cross-entropy loss for the classification:

$$\mathcal{L}_{total} = \mathcal{L}_{ce}(\hat{y}, y) + \frac{1}{K} \sum_{i=1}^K \mathcal{L}_{anchor}^i(\hat{\mathbf{z}}_i, \mathbf{e}_i) \quad (3)$$

## 2.3 Knowledge Guided Prompting

LLMs have a limited ability to make diagnostic decisions with images. Text-based prompting lacks sufficient instructions to guide the LLM in generating high-quality radiology reports. As a result, the LLM hallucinates, producing outputs

that include irrelevant topics and incorrect expressions. Recent methods attempt to bridge semantic gaps by incorporating various types of pre-trained models, such as classification and report generation models. Acquiring these models, especially trained on the same image domain, is challenging. Furthermore, they are also not explainable due to the black-box nature of the neural networks. We propose a novel approach to address LLM hallucinations. Our aim is to consolidate the task of extracting image characteristics into a unified foundation or concept model. Suppose a Vision-Language model comprises a set of visual concept token  $\mathbf{z}_i$  from the visual encoder  $\mathcal{V}$  and diagnostic criteria anchor  $\mathbf{e}_i$  from the textual encoder  $\mathcal{T}$ . Assuming the two sets of tokens are aligned during training, we aim to construct an explainable classifier utilizing their similarity scores. This mirrors the approach of human experts, who make their diagnostic decisions by evaluating the different criteria. We use a linear layer to make the prediction of the final class from these  $K$  similarity scores. The prediction process based on the similarity scores between visual concept tokens and diagnostic criteria anchors is formalized as follows:

$$\hat{y} = W(\text{concat}(\text{sim}(\hat{\mathbf{z}}_1, \mathbf{e}_1), \dots, \text{sim}(\hat{\mathbf{z}}_K, \mathbf{e}_K)))^\top, \quad (4)$$

Where  $\text{concat}(\cdot, \cdot)$  represents the concatenation operation and  $W$  is the weight in the linear layer that reflects the significance of each diagnostic criterion’s contribution towards the overall class prediction. The output provides both the class prediction  $y$  for the image and a set of relevant concepts  $\{\mathbf{e}_i\}_{i=1}^d$ ,  $d \leq K$  offering transparent information about how the model makes the diagnostic decision. Both can be used to augment the prompt. Guiding the model to produce accurate report outputs while minimizing the model complexity.

#### 2.4 Image Based Report Retrieval Augmentation

To further enhance the quality and relevance of the generated reports, we implement an image feature-based RAG pipeline. The purpose of this implementation is analog to a novice practitioner learning how to write the report from both the structure and the content of pre-existing reports of similar tasks. We construct a report database of training images of the following form:

$$\mathcal{Q} = \{(z_i, P_i)\}_{i=1}^{|D|} \quad (5)$$

Where  $(z_i, P_i)$  is a key-value pair where  $z_i$  is the visual concept token for the training image  $x_i$ , and  $P_i$  is the report for the same corresponding image. We precompute and store the visual concept tokens to minimize inference overhead.

Top-K retrieval is a widely used technique in information retrieval. For each image  $x \notin D$ , its visual concept token is matched with each training visual concept token in  $\mathcal{Q}$  using cosine similarity. The reports associated with the top-K matched tokens are retrieved as follows:

$$\mathcal{P}_{\text{retrieve}} = \mathcal{Q}(z_i, z_i \in \text{TopK}_{z \in \{z_1, z_2, \dots, z_{|D|}\}} \text{sim}(z_i, \mathcal{V}(x))) \quad (6)$$

LLM Prompt

```

System Prompt:
You are an expert radiologist with extensive experience in interpreting chest X-rays and writing professional radiology reports. Your task is to generate a clear, concise, and accurate radiology report based on the provided AI model findings and similar reference reports.

User Prompt:
You will receive:
1. AI Model Diagnostic Predictions: Primary diagnoses identified by the model (limited to cardiomegaly, consolidation, atelectasis, effusion, edema, and normal conditions)
2. Detailed Feature Analysis: Systematic breakdown of radiological features including:
  - Heart Size
  - Lung Opacity
  - Location and Distribution of Opacity
  - ...
3. Retrieved Similar Reports: Collection of reference reports from similar cases

# Output Requirements
Generate a radiology report that:
1. Is concise and focused (typically 3-5 sentences)
2. Uses professional radiological terminology and be consistent with the retrieved reports
3. Follows a structured approach:
  - Primary findings first
  - Secondary findings next
  - Additional observations last
4. Follows similar structure and terminology patterns as the retrieved reports
5. Contains no title or conclusion section
6. Use appropriate diagnostic certainty language:
  - Use definitive language only when findings are clear and unambiguous
  - Use qualifying terms like "suggesting," "consistent with", "may reflect", "compatible with", or "cannot exclude" when appropriate
  - State negative findings using terms like "no evidence of", "without", "is not seen"

# Style Guidelines
- Mirror the terminology and phrasing commonly used in the retrieved reports
- Maintain professional medical terminology
- Focus on significant findings
- Be specific about anatomical locations
- Use standard radiological phrases and conventions
- Single paragraph
- No bullet points
- Continuous narrative flow

# Critical Considerations
- Prioritize findings based on clinical significance
- Integrate AI findings with patterns from retrieved reports
- Maintain logical flow from major to minor findings
- Be explicit about the presence or absence of critical findings
- Use consistent terminology throughout the report

```

**Fig. 3.** Prompt template for generating radiology reports.

The information across classification results, explainable concept axis, and top-k example reports are aggregated and incorporated into the prompt for a lightweight knowledge-based prompting. The prompt template is defined in Fig. 3.

## 3 Experiment and Results

### 3.1 Experimental Setup

**Dataset.** We used MIMIC-CXR [12] for a comprehensive evaluation of RadAlign. The dataset contains 377,100 chest X-ray images, including both frontal and lateral chest views. X-rays are stored in JPEG format and with a typical image resolution ranging from  $1000 \times 1000$  pixels. The dataset includes radiology reports for the x-rays, which is a set of descriptions of findings, impressions, and patient history. The dataset provides classes of labels of common findings such

as Atelectasis (AT), Cardiomegaly (CM), Consolidation (CD), Edema (ED) and Pleural Effusion (PE). In our experiments we use 5 of 12 disease classes.

**Baselines.** We evaluate our model against state-of-the-art baselines for both disease classification and report generation tasks. For disease classification, we compare with: PCAM [31], evaluated using both CheXpert-pretrained and MIMIC-CXR-finetuned versions; ChatCAD [27], a finetuned LLM framework; LABO [30], an explainable VLM incorporating concept bottleneck. For report generation, we compare against R2GenCMN [5], which uses cross-modal memory networks for visual-textual integration, and ChatCAD [27].

**Implementation Details.** We prompt GPT-4 to query the diagnostic criteria. We use the pretrained weights of BioViL CLIP Resnet-50 [3]. Our model is implemented with the Bio-ViL specialized. We finetune the model by optimizing only the visual encoder, visual concept tokens, and the final linear layer with AdamW optimizer, while keeping the text encoder fixed. All experiments are conducted using PyTorch with Nvidia RTX 8000 GPUs.

## 3.2 Main Results

**Report Generation Comparison.** We evaluate our model using GREEN Score, a metric specifically designed for assessing medical report generation by leveraging LLM-based reasoning to identify clinically significant errors. Traditional metrics such as BLEU [19], ROUGE [15], and BERTScore [32] are inadequate for medical report evaluation as they only measure surface-level text similarity without considering factual correctness - a critical requirement in clinical contexts where accurately distinguishing between presence and absence of conditions is essential. GREEN offers both quantitative scores and interpretable explanations that align well with expert judgment, as validated through comparisons with medical professionals. For implementation details, we refer readers to the original GREEN Score paper [18].

We present all of the six error notations from the GREEN score evaluations in Table 1, these including (a) False report of a finding in the candidate, (b) Missing a finding present in the reference, (c) Misidentification of a finding’s anatomic location/position, (d) Misassessment of the severity of a finding, (e) Mentioning a comparison that isn’t in the reference, and (f) Omitting a comparison detailing a change from a prior study.

Our experiments demonstrate RadAlign’s superior performance across multiple metrics. Using GPT-4o, RadAlign achieves a GREEN score of 0.678, substantially outperforming the baseline methods (0.634). The improvement is particularly evident in error metrics (b), (c), (e), and (f), indicating better handling of comparative statements while maintaining robust clinical finding identification. The results also reveal distinct scaling behaviors between methods. While ChatCAD shows minimal improvement when upgrading from GPT-4o mini to GPT-4o (0.001 increase), RadAlign demonstrates significant performance gains (0.648

to 0.678). This differential scaling can be attributed to the architectural differences between the approaches. RadAlign’s unified vision-language alignment can leverage the enhanced LLM reasoning capabilities based on the recognized medical concepts, whereas ChatCAD’s multi-model pipeline are not well-aligned and may introduce inconsistency that limit the benefits of more powerful LLMs. The comparable performance between ChatCAD and R2GenCMN can be attributed to ChatCAD’s architectural dependency on R2GenCMN’s output as its LLM input, suggesting limited additive benefits from this pipeline structure.

**Table 1.** Report generation comparison with different radiology report generation methods.

Model	LLM	(a)↓	(b)↓	(c)↓	(d)↓	(e)↓	(f)↓	GREEN ↑
R2GenCMN	-	384	880	18	40	90	17	0.634
ChatCAD	4o-mini	384	884	18	40	92	18	0.633
ChatCAD	4o	384	880	18	40	90	17	0.634
RadAlign (Ours)	4o-mini	645	701	29	55	44	10	0.648
RadAlign (Ours)	4o	701	630	17	54	40	11	<b>0.678</b>

**Classification Accuracy Comparison.** We report disease classification performance in terms of precision, F1 score, AUC for all methods in Table 2, 3 and 4. For report generation methods, after obtaining the output reports from the model, we process them through the CheXpert [10] labeler to automatically assign labels for the five common diseases and then calculate the metrics by comparing the label extracted from the generated reports and the ground truth labels from the dataset.

**Table 2.** Classification results for different methods on precision.

Model	AT	CM	CD	ED	PE	Average
PCAM Pretrain	0.581	0.427	0.503	0.391	0.532	0.487
PCAM	0.616	0.628	0.518	0.546	0.714	0.604
ChatCAD	0.522	0.559	<b>0.533</b>	<b>0.626</b>	0.727	0.593
LABO	0.605	0.613	0.521	0.559	0.682	0.596
RadAlign (Ours)	<b>0.627</b>	<b>0.638</b>	0.525	0.570	<b>0.777</b>	<b>0.627</b>

**Table 3.** Classification results for different methods on the F1 score.

Model	AT	CM	CD	ED	PE	Average
PCAM Pretrain	0.571	0.095	0.029	0.031	0.513	0.248
PCAM	0.618	0.628	0.432	0.514	0.755	0.589
ChatCAD	0.311	0.523	0.527	<b>0.641</b>	0.764	0.553
LABO	0.583	0.607	0.462	0.556	0.714	0.584
RadAlign (Ours)	<b>0.634</b>	<b>0.653</b>	<b>0.473</b>	0.580	<b>0.820</b>	<b>0.632</b>

Our experimental results demonstrate RadAlign’s superior diagnostic classification performance across all metrics, achieving the highest average precision (0.627), F1 score (0.632), and AUC (0.885). Notably, existing methods face significant tradeoffs - ChatCAD, despite using LLMs for report generation, achieves lower classification performance than the specialized classification model PCAM (AUC: 0.683 vs 0.861). Similarly, explainable models like LABO underperform compared to black-box approaches. In contrast, RadAlign achieves state-of-the-art classification accuracy while maintaining strong report generation capabili-

**Table 4.** Classification results for different methods on AUC.

Model	AT	CM	CD	ED	PE	Average
PCAM Pretrain	0.722	0.299	0.383	0.137	0.565	0.421
PCAM	0.838	<b>0.876</b>	0.787	0.868	0.937	0.861
ChatCAD	0.542	0.650	0.724	0.662	0.838	0.683
LABO	0.753	0.768	0.747	0.820	0.847	0.787
RadAlign (Ours)	<b>0.853</b>	0.873	<b>0.824</b>	<b>0.924</b>	<b>0.954</b>	<b>0.885</b>

**Fig. 4.** Two case studies from the LLM prediction, report reference from human radiologist, and the GREEN evaluation. RadAlign demonstrates a thorough understanding of the diagnostic and outputs more descriptions than the radiologist reports.

ties and model explainability. This superiority can be attributed to our model’s effective alignment between visual features and medical concepts, enabling accurate diagnosis without sacrificing interpretability or reporting quality.

**Qualitative Evaluation.** We present two representative test cases in Fig. 4 to demonstrate RadAlign’s report generation quality. Our model generates comprehensive reports that systematically document both normal and abnormal findings using standardized terminology. While radiologist references often focus primarily on abnormalities, RadAlign’s concept-based approach ensures thorough coverage of all anatomical structures, aligning with clinical reporting guidelines [21]. The GREEN evaluation confirms these detailed reports maintain accuracy while providing valuable documentation for clinical decision support.

### 3.3 Ablation Studies

**Evaluation with different LLMs.** To evaluate the generalizability of our approach, we test RadAlign with various LLMs including ChatGPT (3.5-Turbo,

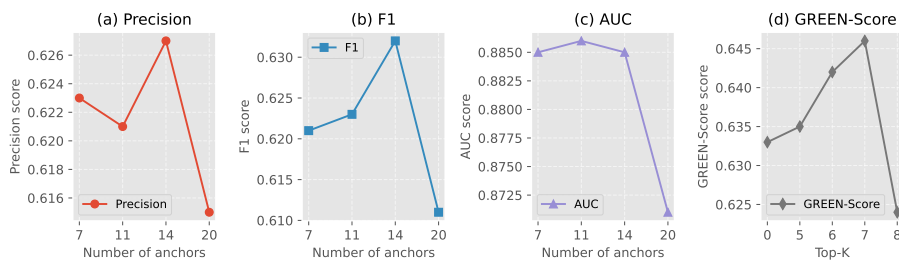


**Fig. 5.** (a), (b), (c) shows classification performance in precision, F1 and AUC given the number of concept anchors. (d) shows the GREEN-score when retrieving  $K$  most similar reports from the train set.

4o-mini, 4o), Claude 3.5-Sonnet, and Llama 3.1, see in Table 5. Notably, all variants achieve GREEN scores (0.646-0.695) surpassing previous baselines (0.634), demonstrating that our concept-based alignment approach is robust across different LLM architectures. We observe consistent performance improvements with more advanced models (ChatGPT 3.5: 0.648  $\rightarrow$  4o: 0.678), suggesting that stronger reasoning capabilities enhance report generation quality when properly grounded in visual concepts. Interestingly, Llama 3.1 achieves the highest score (0.695) despite its smaller size, indicating that efficient model architectures combined with effective visual-concept alignment can outperform larger models for specialized medical tasks.

**Table 5.** Report generation performance of RadAlign with different LLMs.

LLM	(a) $\downarrow$	(b) $\downarrow$	(c) $\downarrow$	(d) $\downarrow$	(e) $\downarrow$	(f) $\downarrow$	GREEN $\uparrow$
ChatGPT 3.5-Turbo	733	668	17	54	57	12	0.648
ChatGPT 4o-mini	645	701	29	55	44	10	0.646
ChatGPT 4o	701	630	17	54	40	11	0.678
Claude 3.5-Sonnet	749	651	11	63	48	8	0.658
Llama 3.1	560	624	14	40	51	12	0.695

**Number of Concept Anchors.** Our experiments show that model performance peaks with 14 concept anchors across most metrics (precision, F1, and AUC) as shown in Fig. 5 (a-c). Additional concepts beyond this point degrade performance, suggesting that excessive concepts may introduce noise rather than meaningful features for diagnosis.

**Report retrieval number  $K$ .** Another hyper-parameter is the number of top similar reports for Report Retrieval Augmentation. We use linear search for the optimal  $K$  and find  $K = 7$  to yield the best GREEN-Score, as shown in Fig. 5 (d). Performance improves initially as retrieved validated historical reports provide better semantic alignment but degrades with larger  $K$  as unrelated cases introduce noise. This demonstrates the importance of balanced retrieval in guiding LLM-based report generation.

**Vision Encoder Architecture.** Our model shows consistent performance across both ResNet50 [9] and ViT-Base [8] architectures (Table 6), indicating our concept alignment approach is robust to visual encoder architectures.

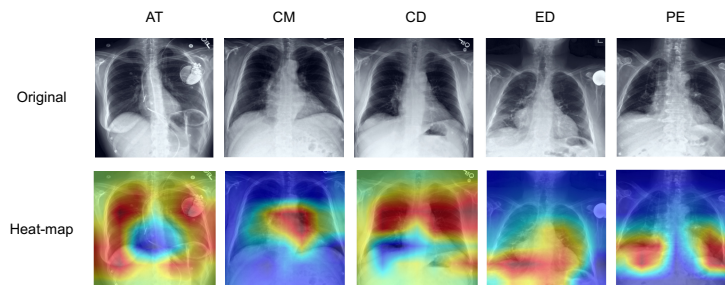


**Fig. 6.** Heatmap visualization of the attention weight from the visual concept token. Warmer color indicates higher attention scores from the model, and cooler color indicates lower attention scores from the model. (Best view in color)

**Table 6.** Classification results of our method when changing different vision backbones on the F1 score.

Visual encoder	AT	CM	CD	ED	PE	Average
ResNet50	0.587	0.611	0.469	0.548	0.803	0.604
ViT-Base	0.651	0.646	0.477	0.540	0.819	0.627

### 3.4 Concept Interpretation

RadAlign enables interpretation of its decision-making process through visualization of concept token attention weights, demonstrating disease-specific localization patterns that align with clinical expertise. As shown in Fig. 6, the attention heatmaps highlight anatomically relevant regions for each condition. For example, for disease class Atelectasis (AT), the heatmap highlights specific areas around the edge of the lung fields that are indicative of abnormalities, while for class Cardiomegaly (CM), attention is drawn to distinct location at the heart region. These visualizations not only validate that our concept tokens successfully capture clinically meaningful features, but also provide radiologists with transparent insight into the model’s reasoning process. Such interpretability helps verify that the model’s decisions are based on relevant medical features rather than spurious correlations, making the automated analysis more trustworthy for clinical radiology workflows.

## 4 Conclusion

In this paper, we present RadAlign, a novel framework that addresses critical challenges in automated radiology report generation by combining the strengths



of predictive and generative AI. Our approach aligns visual features with medical concepts through specialized VLMs and leverages LLMs’ strong reasoning capabilities, achieving superior performance in both disease classification and report generation. The retrieval-augmented generation mechanism, inspired by the radiologist workflow, grounds model outputs in similar historical cases, significantly reducing hallucination while maintaining interpretability. Through comprehensive evaluation, RadAlign demonstrates that combining concept-aligned visual understanding with large language models can achieve both diagnostic accuracy and reliable reporting, representing a significant advance in interpretable medical AI. While these results show promising progress toward clinically reliable automation, future work will focus on refining concept formulation to better capture complex medical knowledge and further enhance diagnostic accuracy.

## References

1. Anderson, P., He, X., Buehler, C., Teney, D., Johnson, M., Gould, S., Zhang, L.: Bottom-up and top-down attention for image captioning and visual question answering. In: Proceedings of the IEEE conference on computer vision and pattern recognition. pp. 6077–6086 (2018)
2. Asif, S., Wenhui, Y., Jin, H., Jinhai, S.: Classification of covid-19 from chest x-ray images using deep convolutional neural network. In: 2020 IEEE 6th international conference on computer and communications (ICCC). pp. 426–433. IEEE (2020)
3. Boecking, B., Usuyama, N., Bannur, S., Castro, D.C., Schwaighofer, A., Hyland, S., Wetscherek, M., Naumann, T., Nori, A., Alvarez-Valle, J., et al.: Making the most of text semantics to improve biomedical vision–language processing. In: European conference on computer vision. pp. 1–21. Springer (2022)
4. Brown, T., Mann, B., Ryder, N., Subbiah, M., Kaplan, J.D., Dhariwal, P., Neelakantan, A., Shyam, P., Sastry, G., Askell, A., et al.: Language models are few-shot learners. *Advances in neural information processing systems* **33**, 1877–1901 (2020)
5. Chen, Z., Shen, Y., Song, Y., Wan, X.: Cross-modal memory networks for radiology report generation. arXiv preprint arXiv:2204.13258 (2022)
6. Chen, Z., Song, Y., Chang, T.H., Wan, X.: Generating radiology reports via memory-driven transformer. arXiv preprint arXiv:2010.16056 (2020)
7. Devlin, J.: Bert: Pre-training of deep bidirectional transformers for language understanding. arXiv preprint arXiv:1810.04805 (2018)
8. Dosovitskiy, A., Beyer, L., Kolesnikov, A., Weissenborn, D., Zhai, X., Unterthiner, T., Dehghani, M., Minderer, M., Heigold, G., Gelly, S., et al.: An image is worth 16x16 words: Transformers for image recognition at scale. arXiv preprint arXiv:2010.11929 (2020)
9. He, K., Zhang, X., Ren, S., Sun, J.: Deep residual learning for image recognition. In: Proceedings of the IEEE conference on computer vision and pattern recognition. pp. 770–778 (2016)
10. Irvin, J., Rajpurkar, P., Ko, M., Yu, Y., Ciurea-Ilcus, S., Chute, C., Marklund, H., Haghighi, B., Ball, R., Shpanskaya, K., et al.: Chexpert: A large chest radiograph dataset with uncertainty labels and expert comparison. In: Thirty-Third AAAI Conference on Artificial Intelligence (2019)
11. Jing, B., Wang, Z., Xing, E.: Show, describe and conclude: On exploiting the structure information of chest x-ray reports. arXiv preprint arXiv:2004.12274 (2020)

- 14 Difei Gu, Yunhe Gao, Yang Zhou, Mu Zhou, and Dimitris Metaxas
13. Johnson, A.E., Pollard, T.J., Berkowitz, S.J., Greenbaum, N.R., Lungren, M.P., Deng, C.y., Mark, R.G., Horng, S.: Mimic-cxr, a de-identified publicly available database of chest radiographs with free-text reports. *Scientific data* **6**(1), 317 (2019)
  14. Li, J., Li, D., Savarese, S., Hoi, S.: Blip-2: Bootstrapping language-image pre-training with frozen image encoders and large language models. In: *International conference on machine learning*. pp. 19730–19742. PMLR (2023)
  15. Li, Y., Liang, X., Hu, Z., Xing, E.P.: Hybrid retrieval-generation reinforced agent for medical image report generation. *Advances in neural information processing systems* **31** (2018)
  16. Lin, C.Y.: ROUGE: A package for automatic evaluation of summaries. In: *Text Summarization Branches Out*. pp. 74–81. Association for Computational Linguistics, Barcelona, Spain (Jul 2004), <https://aclanthology.org/W04-1013>
  17. McBee, M.P., Awan, O.A., Colucci, A.T., Ghobadi, C.W., Kadom, N., Kansagra, A.P., Tridandapani, S., Auffermann, W.F.: Deep learning in radiology. *Academic radiology* **25**(11), 1472–1480 (2018)
  18. Okolo, G.I., Katsigiannis, S., Ramzan, N.: Ievit: An enhanced vision transformer architecture for chest x-ray image classification. *Computer Methods and Programs in Biomedicine* **226**, 107141 (2022)
  19. Ostmeier, S., Xu, J., Chen, Z., Varma, M., Blankemeier, L., Bluethgen, C., Michalson, A.E., Moseley, M., Langlotz, C., Chaudhari, A.S., et al.: Green: Generative radiology report evaluation and error notation. *arXiv preprint arXiv:2405.03595* (2024)
  20. Papineni, K., Roukos, S., Ward, T., Zhu, W.J.: Bleu: a method for automatic evaluation of machine translation. In: *Proceedings of the 40th annual meeting of the Association for Computational Linguistics*. pp. 311–318 (2002)
  21. Park, S., Kim, G., Oh, Y., Seo, J.B., Lee, S.M., Kim, J.H., Moon, S., Lim, J.K., Park, C.M., Ye, J.C.: Self-evolving vision transformer for chest x-ray diagnosis through knowledge distillation. *Nature communications* **13**(1), 3848 (2022)
  22. Pesapane, F., Tantrige, P., De Marco, P., Carriero, S., Zugni, F., Nicosia, L., Bozzini, A.C., Rotili, A., Latronico, A., Abbate, F., et al.: Advancements in standardizing radiological reports: a comprehensive review. *Medicina* **59**(9), 1679 (2023)
  23. Radford, A., Kim, J.W., Hallacy, C., Ramesh, A., Goh, G., Agarwal, S., Sastry, G., Askell, A., Mishkin, P., Clark, J., et al.: Learning transferable visual models from natural language supervision. In: *ICML*. pp. 8748–8763. PMLR (2021)
  24. Ramesh, V., Chi, N.A., Rajpurkar, P.: Improving radiology report generation systems by removing hallucinated references to non-existent priors. In: *Machine Learning for Health*. pp. 456–473. PMLR (2022)
  25. Reale-Nosei, G., Amador-Domínguez, E., Serrano, E.: From vision to text: A comprehensive review of natural image captioning in medical diagnosis and radiology report generation. *Medical Image Analysis* p. 103264 (2024)
  26. Touvron, H., Lavril, T., Izacard, G., Martinet, X., Lachaux, M.A., Lacroix, T., Rozière, B., Goyal, N., Hambro, E., Azhar, F., et al.: Llama: Open and efficient foundation language models. *arXiv preprint arXiv:2302.13971* (2023)
  27. Vinyals, O., Toshev, A., Bengio, S., Erhan, D.: Show and tell: A neural image caption generator. In: *Proceedings of the IEEE conference on computer vision and pattern recognition*. pp. 3156–3164 (2015)
  28. Wang, S., Zhao, Z., Ouyang, X., Wang, Q., Shen, D.: Chatcad: Interactive computer-aided diagnosis on medical image using large language models. *arXiv preprint arXiv:2302.07257* (2023)

28. Wang, Z., Liu, L., Wang, L., Zhou, L.: R2gengpt: Radiology report generation with frozen llms. *Meta-Radiology* **1**(3), 100033 (2023)
29. Wang, Z., Wu, Z., Agarwal, D., Sun, J.: Medclip: Contrastive learning from unpaired medical images and text. arXiv preprint arXiv:2210.10163 (2022)
30. Yang, Y., Panagopoulou, A., Zhou, S., Jin, D., Callison-Burch, C., Yatskar, M.: Language in a bottle: Language model guided concept bottlenecks for interpretable image classification. In: *Proceedings of the IEEE/CVF Conference on Computer Vision and Pattern Recognition*. pp. 19187–19197 (2023)
31. Ye, W., Yao, J., Xue, H., Li, Y.: Weakly supervised lesion localization with probabilistic-cam pooling. arXiv preprint arXiv:2005.14480 (2020)
32. Zhang, T., Kishore, V., Wu, F., Weinberger, K.Q., Artzi, Y.: Bertscore: Evaluating text generation with bert. arXiv preprint arXiv:1904.09675 (2019)